Reflectance of acoustic horns and solution of the inverse problem

Daniel M. Rasetshwane[a) and Stephen T. Neely
Boys Town National Research Hospital, 555 North 30th Street, Omaha, Nebraska 68131

Jont B. Allen
Department of Electrical and Computer Engineering, University of Illinois at Urbana-Champaign, Urbana, Illinois 61801

Christopher A. Shera
Eaton-Peabody Laboratories, Massachusetts Eye and Ear Infirmary, Boston, Massachusetts 02114

A method is described for solving the inverse problem of determining the profile of an acoustic horn when time-domain reflectance (TDR) is known only at the entrance. The method involves recasting Webster's horn equation in terms of forward and backward propagating wave variables. An essential feature of this method is a requirement that the backward propagating wave be continuous at the wave-front at all locations beyond the entrance. Derivation of the inverse solution raises questions about the meaning of causality in the context of wave propagation in non-uniform tubes. Exact reflectance expressions are presented for infinite exponential, conical and parabolic horns based on exact solutions of the horn equation. Diameter functions obtained with the inverse solution are a good match to all three horn profiles. © 2012 Acoustical Society of America.
[DOI: 10.1121/1.3681923]

I. INTRODUCTION

A horn is a tapered sound guide consisting of a tube of varying cross-sectional area. The efficiency or performance of a horn as an acoustical transporter is routinely measured using impedance. By solving Webster's horn equation (Webster, 1919), theoretical equations for impedance have been derived for several common cross-sectional area functions. This problem is referred to as the *direct problem*. The *inverse problem* determines the area function from acoustical measurements made at one end of the horn. For a review of the theory of horns see Eisner (1967).

This paper describes a solution to the inverse problem that calculates an area function from reflectance for infinite-length acoustic horns. An essential part of the derivation of this solution is having a definition of reflectance that is compatible with the solution. Our numerical method accurately determines horn area as a function of axial distance given only reflectance at the horn entrance. Formulating the inverse-solution method in terms of reflectance offers a new perspective on the meaning of reflectance, impedance, and causality. A better understanding of these issues may be useful when measuring impedance and reflectance in the laboratory and when interpreting these measurements.

Salmon (1946) obtained a solution to the inverse problem that relates acoustic impedance to the shape of a family of horns derived from the exponential horn. He showed that some impedance functions do not result in realizable horns of this family. Consequently, his solution to the inverse problem is limited since it cannot be used to obtain an area function from an arbitrary impedance function.

Schroeder (1967) described an inverse solution for determining the shape of the vocal tract from measurements of resonant frequencies (formant frequencies). He used perturbation theory based on the assumption that a small change in the energy of an oscillator causes a small change in the frequency of oscillation to relate the change in energy for one of the modes of an acoustic pipe to the change in area of the pipe and acoustic radiation pressure. The change in area was expanded into a Fourier cosine series and some boundary conditions were assumed for the radiation pressure to shows that the Fourier series coefficients of the area function can be determined from the resonance frequencies. These coefficients were used in the calculation of the area function. Since only odd coefficients were allowed and the number of modes used in the calculations of area function were limited, the spatial resolution of Schroeder's area estimation was low and the correspondence to known fixed area functions was only fair. Schroeder suggested that the performance of his method can be improved by including measurements of impedance functions at the lip.

Mermelstein (1967) extended the work of Schroeder (1967) and showed that the inclusion of the impulse response in the determination of the shape of the vocal tract does indeed improve the estimation of the area function. This inclusion also makes the determined area function unique. In Schroeder's method, the formant frequencies correspond to the odd terms of the Fourier coefficients of the area function. The zeros of the admittance function of the impulse response correspond to the even terms of the Fourier coefficients. This additional information is responsible for the improvement in the estimation of the area function.

a)Author to whom correspondence should be addressed. Electronic mail: daniel.rasetshwane@boystown.org.

Sondhi and Gopinath (1971) proposed a solution to the inverse problem for determining the shape of the vocal tract from measurements of an impulse response. Their solution starts with Webster's horn equation relating pressure $p(x,t)$, volume velocity $u(x,t)$ and cross-sectional area $A(x)$ using first order differential equations. They assume quiescence at $t = t_0$, that is, $p(x,t_0) = 0$ and $u(x,t_0) = 0$, and then reduce Webster's horn equations to an expression that relates volume velocity at the lips $(x = 0)$ to a product of the area function and pressure:

$$V(a) \equiv \int_{t_0}^{t_0+a/c} u(0,t)dt = \int_0^a A(x)p(x, t_0 + a/c)dx, \quad (1)$$

where c is the speed of sound. If for every a one could determine an input $u(0, t)$ such that $p(x, t_0 + a/c) = 1$ for $0 \leq x \leq a$, the right hand side of Eq. (1) would become equal to the volume of the vocal tract up to $x = a$, $V(a)$. Thus the volume $V(a)$ and hence the area function $A(a)$ would be determined as a function of a. Sondhi and Gopinath showed that such input indeed exists and can be determined from knowledge of the impulse response alone. Based on this analysis, they derived an expression that relates the volume velocity at $x = a$ to the impulse response of the vocal tract $h(t)$:

$$u(a,t) + \frac{1}{2}\int_{-a/c}^{a/c} h(|t - \tau|)u(a,\tau)d\tau = 1, |t| \leq a/c. \quad (2)$$

Equation (2) may also be expressed in operator notation as

$$(I + H_a)u(a,t) = 1, \quad (3)$$

where I is the identity operator and H_a is the integral operator with the symmetric kernel $\frac{1}{2}h(|t - \tau|)$. Sondhi and Gopinath showed that $I + H_a$ is positive definite and thus has an inverse that is unique. If $h(t)$ is known, a solution for $u(a,t)$ can be obtained by inverting Eq. (3), and in turn a solution for $V(a)$ can also be obtained from Eq. (1). Differentiation of $V(a)$ yields the area function $A(a)$. Experimental results showed that their method can accurately determine the area function of non-uniform tubes.

Caflisch (1981) formulated a solution to the inverse problem to obtain the capacitance taper of a discrete transmission line from the impulse response (voltage) of the line. His method is a discrete-time version of a continuous-time method described by Sondhi and Gopinath (1971). Caflisch started with the telegrapher's equations (an electrical analogue of the horn equation) and constructed a Toeplitz matrix whose first column is a function of the voltage of the transmission line in response to a forcing impulse of current. The capacitance taper is then obtained from the central mass sequence of the Toeplitz matrix. Although Caflisch's method reproduces accurate area functions from time-domain impedances, it does not invert time-domain reflectances and is unsuitable when impedances are well-known only in the frequency-domain, such as in the case of infinite-length horns.

Sondhi and Resnick (1983) described numerical procedures and experiments for estimating vocal tract area functions using the inverse solution of Sondhi and Gopinath (1971) from time-domain impedance and step reflectance, a time integral of reflectance. However, results presented showed only a fair match to known area functions and a poor match for area functions with constrictions.

Bube and Burridge (1983) described a solution to the inverse problem for obtaining mechanical properties of the earth deep underground from measurements of particle motion at the surface. Their method was also inspired by and extends the method of Sondhi and Gopinath (1971). Bube and Burridge start with the isotropic elasticity equations (a hyperbolic system of differential equations relating pressure and particle velocity as functions of time and depth into the ground for an isotropic medium) and then pose the inverse problem as that of finding the coefficients of the differential equations (depth-dependent characteristic impedance) given initial and boundary data. They formulated their solution in the continuum domain and then obtain several corresponding discrete versions. Bube and Burridge discussed the accuracy of their method and pointed out that it is limited by the discretization step and that it is exact only for layered media in which the properties of the material are homogeneous across each layer. The assumption of homogeneous layered media is also a feature of the methods of Caflisch, and Sondhi and Resnick, and is reminiscent of the Bremmer (1951) series solution of the wave equation.

Milenkovic (1987) considered an acoustic tube to be made up of a concatenation of uniform tubes and that the acoustic pressure signal in each of these tubes can be separated into forward and backward traveling wave components. The separation of the total acoustic pressure into the wave components was done using an autoregressive-moving average. The wave components in each tube were represented using a z-transform. The sampling rate of the acoustic signal was relative to the length of the intermediate acoustic tube elements so that the z-transform delay operator $z^{-1/2}$ represented the sound propagation time for sound to traverse one tube section. If both the number of tube sections and the sampling rate are high enough, his method can be used to approximate a tube of continuously varying cross section. In order to allow his system to have non-causal input, Milenkovic used a filter that transforms a non-causal system to a causal system. The coefficients of this filter were calculated using a least-square criterion. The ability to use a non-casual input allowed for the formulation of an inverse solution that does not assume zero-initial conditions.

Amir et al. (1995) described a solution to the inverse problem that is similar to that of Milenkovic (1987). Like the latter, they considered an acoustic tube to be made up of a concatenation of cylindrical segments, decomposed acoustic pressure in each segment into forward and backward traveling wave components, and assumed that reflections only occur at the junction of two segments. They extended their method to conical segments and to account for propagation losses. Their method has been applied in reflectometry, a non-invasive measurement of the cross-section area of non-uniform ducts (e.g., Forbes et al., 2003). However, their method requires a high bandwidth to produce a good spatial resolution, which is a confound for reflectometry since the

source tube used in the measurement equipment severely limits bandwidth.

The presentation of our solution to the inverse problem begins with the recasting of Webster's horn equation in terms of forward and backward traveling pressure waves. The wave variables are obtained through decomposition of the total acoustical pressure. This is followed by a second definition of reflectance that is compatible with the solution, but not necessarily causal. Then the inverse solution itself is described. The solution to the inverse problem is applied to infinite parabolic, conical and exponential horns. Our approach of starting the formulation of the solution to the inverse problem with Webster's horn equation is similar to that of Sondhi and Gopinath (1971), while our use of pressure wave variables in the formulation is similar to that of Milenkovic (1987) and Amir et al. (1995). Our treatment of acoustic horns with known exact solutions is novel and focus attention on the accuracy of the inverse solution. Our solution method has the potential of being adapted to practical measurement situations; however, its derivation raises theoretical questions about the meaning of reflectance in non-uniform horns.

II. ANALYSIS

A. Webster's horn equation

Under the assumption of lossless plane-wave propagation in a tube of variable cross-sectional area $A(x)$, the equations relating acoustic pressure $p(x,t)$ and volume velocity $u(x,t)$ are

$$\partial_x p = -\frac{\rho}{A(x)}\partial_t u, \tag{4}$$

$$\partial_x u = -\frac{A(x)}{\rho c^2}\partial_t p, \tag{5}$$

where ρ is the density of air and c is the speed of sound (Webster, 1919). This relation is known as the *horn equation*.

Equations (4) and (5) may be combined to eliminate u and produce a second-order equation in p:

$$\partial_x^2 p + 2\varepsilon(x)\partial_x p - \frac{1}{c^2}\partial_t^2 p = 0, \tag{6}$$

where

$$\varepsilon(x) \equiv \frac{1}{2}\frac{d}{dx}\ln A(x), \tag{7}$$

is the logarithmic gradient of the horn diameter.

We seek a formulation of the horn equation that leads to a solution of the inverse problem. Specifically, given the boundary condition $p(0,t)$, $u(0,t)$, and $A(0)$ for $t \geq 0$ and the initial condition that $p(x,0) = u(x,0) = 0$ for $x > 0$, we want to calculate $A(x)$ for $x > 0$. Our approach will be to decompose $p(x,t)$ into *wave variables* that represent pressure waves traveling in two directions.

B. Reflectance

We start by deriving expressions for the forward and backward travelling wave variables $p_+(x,t)$ and $p_-(x,t)$ that satisfy two expected properties: (1) superposition and (2) causality. The superposition requirement is simply that their sum is the total pressure:

$$p(x,t) = p_+(x,t) + p_-(x,t). \tag{8}$$

The causality requirement is that the deconvolution of $p_-(x,t)$ by $p_+(x,t)$, which we will call *reflectance*, is zero for $t < 0$ and $x = 0$. However, our inverse solution imposes a different restriction on reflectance at locations for $x > 0$. Instead of causality, the requirement for $x > 0$ is that reflectance is zero at $t = 0$. This requirement becomes important because non-uniform tubes have an inertial component in their radiation admittance that creates a time-domain step in reflectance at $t = 0$. Our inverse solution requires a definition of reflectance that eliminates this discontinuity.

It is convenient to define reflectance in the frequency domain as a transfer function:

$$R(x,\omega) \equiv \frac{P_-(x,\omega)}{P_+(x,\omega)}, \tag{9}$$

where $P_+(x,\omega)$ and $P_-(x,\omega)$ are the Fourier transforms of $p_+(x,t)$ and $p_-(x,t)$.

In a uniform tube, $p_+(x,t)$ and $p_-(x,t)$ are not coupled to each other by the horn equation. In this case, the ratio of $p_+(x,t)$ and $p_-(x,t)$ is usually called the *reflection coefficient* and may be expressed as

$$R_1(x,\omega) = \frac{Y_0(x) - Y_r(x,\omega)}{Y_0(x) + Y_r(x,\omega)}, \tag{10}$$

where the *radiation admittance* is defined as

$$Y_r(x,\omega) \equiv \frac{U(x,\omega)}{P(x,\omega)} \tag{11}$$

(e.g., Keefe et al., 1992). We refer to Eq. (10) as Type-I reflectance. In Eq. (11), $P(x,\omega)$ and $U(x,\omega)$ are Fourier transforms of $p(x,t)$ and $u(x,t)$. In Eq. (10), the *surge admittance*, which is also known as the *characteristic admittance*, may be calculated from the radiation admittance:

$$Y_0(x) = \lim_{\omega \to \infty} \frac{1}{2\omega}\int_{-\omega}^{\omega} Y_r(x,\omega)d\omega. \tag{12}$$

The radiation and surge admittances may be determined experimentally from measurements of $P(x,\omega)$ and $U(x,\omega)$. In terms of the general horn equation, $Y_0(x) = A(x)/\rho c$. In a uniform tube, $Y_0 = A_0/\rho c$ is a constant, independent of x.

In a non-uniform acoustic horn, an inverse Fourier transform of the RHS of Eq. (10) may become non-zero at $t = 0$ due to the reactive component of Y_r. In order to restore continuity in the time-domain, we introduce the following expression as our definition of *reflectance*:

J. Acoust. Soc. Am., Vol. 131, No. 3, March 2012

Rasetshwane et al.: Horn inverse solution   1865

$$R_2(x,\omega) = \frac{Y_0(x) - [Y_r(x,\omega) - Y_s(x,\omega)]}{Y_0(x) + [Y_r(x,\omega) - Y_s(x,\omega)]}. \tag{13}$$

Subtraction of Y_s from Y_r restores continuity in the time-domain by removing the step at $t = 0$ for all horn shapes. We were surprised that accurate inverse solutions are obtained even for the parabolic horn, where removal of the time-domain step creates a non-causal reflectance. We refer to Eq. (13) as Type-II reflectance. The quantity Y_s is called the *step admittance* because of its time-domain properties and is defined by the following expression:

$$Y_s(x,\omega) \equiv Y_0(x)\frac{c}{i\omega}b(x), \tag{14}$$

where

$$b(x) = \lim_{\omega \to \infty}\frac{i\omega}{c}\left[\frac{Y_r(x,\omega)}{Y_0(x)} - 1\right]. \tag{15}$$

However, at $x = 0$, we require that reflectance is causal. To incorporate both types of reflectance into a single definition, we will use the following expression for reflectance for the purpose of defining wave variables:

$$R(x,\omega) = \frac{Y_0(x) - \left[Y_r(x,\omega) - Y_0(x)\frac{c}{i\omega}B(x)\right]}{Y_0(x) + \left[Y_r(x,\omega) - Y_0(x)\frac{c}{i\omega}B(x)\right]}. \tag{16}$$

In this equation, we will set $B(0) = 0$ at $x = 0$ to represent Type-I reflectance and ensure causality; however, we will set $B(x) = b(x)$ when $x > 0$ to represent Type-II reflectance and ensure continuity at $t = 0$. We refer to $b(x)$ as the *horn inertance* because it has properties that are similar to the inertance defined by Olson (1947).

C. Wave variables

The following definitions of $P_+(x,\omega)$ and $P_-(x,\omega)$ are derived by comparing Eq. (16) with the definition of reflectance in Eq. (9):

$$P_+(x,\omega) = \frac{1}{2}\left\{P(x,\omega)\left[1 - \frac{c}{i\omega}B(x)\right] + \frac{U(x,\omega)}{Y_0(x)}\right\}, \tag{17}$$

$$P_-(x,\omega) = \frac{1}{2}\left\{P(x,\omega)\left[1 + \frac{c}{i\omega}B(x)\right] - \frac{U(x,\omega)}{Y_0(x)}\right\}. \tag{18}$$

The corresponding wave variables in the time domain are described by the following equations:

$$p_+(x,t) = \frac{1}{2}\left\{p(x,t) + \left[\frac{u(x,t)}{Y_0(x)} - cB(x)\int_0^t p(x,t)dt\right]\right\}, \tag{19}$$

$$p_-(x,t) = \frac{1}{2}\left\{p(x,t) - \left[\frac{u(x,t)}{Y_0(x)} - cB(x)\int_0^t p(x,t)dt\right]\right\}. \tag{20}$$

Note that, as required for superposition,

$$p_+(x,t) + p_-(x,t) = p(x,t), \tag{21}$$

and that

$$p_+(x,t) - p_-(x,t) = \frac{u(x,t)}{Y_0(x)} - cB(x)\int_0^t p(x,t)dt. \tag{22}$$

The definition of $b(x)$ in Eq. (15) guarantees that

$$\lim_{\omega \to \infty}i\omega P_-(x,\omega) = 0, \tag{23}$$

for $x > 0$. Likewise, in the time domain, the definition of $b(x)$ and the initial value theorem guarantee that

$$\lim_{t \to 0}p_-(x,t + x/c) = 0, \tag{24}$$

for $x > 0$. The inverse solution takes advantage of this property to calculate values for $b(x)$ when $x > 0$. This property also ensures that $p_-(x,t + x/c) = 0$ for $t < 0$ and $x > 0$, provided that the boundary condition at $x = 0$ is causal.

D. Wave-variable horn equation

We want to express Webster's horn equation in terms of the wave variables $p_+(x,t)$ and $p_-(x,t)$. We start by examining partial derivatives of Eqs. (19) and (20) with respect to x:

$$\partial_x p_+ = \frac{1}{2}\left\{\partial_x p + \left[Z_0 \cdot \partial_x u + \partial_x Z_0 \cdot u - cB \cdot \int_0^t \partial_x p dt\right.\right.$$
$$\left.\left. - c\partial_x B \cdot \int_0^t p dt\right]\right\}, \tag{25}$$

$$\partial_x p_- = \frac{1}{2}\left\{\partial_x p - \left[Z_0 \cdot \partial_x u + \partial_x Z_0 \cdot u - cB \cdot \int_0^t \partial_x p dt\right.\right.$$
$$\left.\left. - c\partial_x B \cdot \int_0^t p dt\right]\right\}, \tag{26}$$

where $Z_0 = 1/Y_0$. We use Eq. (4) to simplify the first integral on the RHS of Eqs. (25) and (26):

$$\partial_x p_+ = \frac{1}{2}\left\{\partial_x p + \left[Z_0 \cdot \partial_x u + \partial_x Z_0 \cdot u - B \cdot Z_0 u\right.\right.$$
$$\left.\left. - c\partial_x B \cdot \int_0^t p dt\right]\right\}, \tag{27}$$

$$\partial_x p_- = \frac{1}{2}\left\{\partial_x p - \left[Z_0 \cdot \partial_x u + \partial_x Z_0 \cdot u - B \cdot Z_0 u\right.\right.$$
$$\left.\left. - c\partial_x B \cdot \int_0^t p dt\right]\right\}. \tag{28}$$

We continue by examining partial derivatives of p_+ and p_- with respect to t:

$$\partial_t p_+ = \frac{1}{2}\{\partial_t p + [Z_0 \cdot \partial_t u - cB \cdot p]\}, \tag{29}$$

$$\partial_t p_- = \frac{1}{2}\{\partial_t p - [Z_0 \cdot \partial_t u - cB \cdot p]\}. \tag{30}$$

We use Eqs. (4) and (5) to replace the time derivatives on the RHS of Eqs. (29) and (30) with spatial derivatives:

$$\partial_t p_+ = -\frac{1}{2}c\{Z_0 \cdot \partial_x u + [\partial_x p + B \cdot p]\}, \tag{31}$$

$$\partial_t p_- = -\frac{1}{2}c\{Z_0 \cdot \partial_x u - [\partial_x p + B \cdot p]\}. \tag{32}$$

Combining Eqs. (27) and (28) with Eqs. (31) and (32) gives the following result:

$$\left[\partial_x + \frac{1}{c}\partial_t\right]p_+ = -\frac{1}{2}Bp - \left[\left(\varepsilon - \frac{1}{2}B\right) \cdot \frac{u}{Y_0} + \eta \cdot \int_0^t p\,dt\right], \tag{33}$$

$$\left[\partial_x - \frac{1}{c}\partial_t\right]p_- = -\frac{1}{2}Bp + \left[\left(\varepsilon - \frac{1}{2}B\right) \cdot \frac{u}{Y_0} + \eta \cdot \int_0^t p\,dt\right], \tag{34}$$

where ε was defined in Eq. (7) and

$$\eta(x) \equiv \frac{c}{2}\frac{d}{dx}B(x). \tag{35}$$

Equations (33) and (34) represent Webster's horn equation as a pair of directional derivatives operating on p_+ and p_-. A corresponding pair of line integrals along the paths described by these directional derivatives may offer a potential solution to the horn equation.

E. Inverse solution

We want to solve for $A(x)$ for $x > 0$ given p_+, p_-, A, and B at $x = 0$. We begin by considering a finite-difference approximation of Eqs. (33) and (34):

$$\frac{p_+(x_{n+1}, t_{m+1}) - p_+(x_n, t_m)}{c\Delta t} \approx -B_n p_{nm} \\ - [(\varepsilon_n - B_n)u_{nm} + \eta_n q_{nm}], \tag{36}$$

$$\frac{p_-(x_{n+1}, t_{m-1}) - p_-(x_n, t_m)}{c\Delta t} \approx -B_n p_{nm} \\ - [(\varepsilon_n - B_n)u_{nm} + \eta_n q_{nm}], \tag{37}$$

where n and m are integers, $x_n = nc\Delta t$, $t_m = m\Delta t$, $B_n = \frac{1}{2}B(x_n)$, $p_{nm} = p(x_n, t_m)$, $u_{nm} = u(x_n, t_m)/Y_0(x_n)$, $\varepsilon_n = \varepsilon(x_n)$, $\eta_n = \eta(x_n)$, and $q_{nm} = \Delta t \sum_{v=0}^{m} p(x_n, t_v)$. We need a procedure to calculate p_+, p_-, and A at $x = x_{n+1}$ given these variables at $x = x_n$.

The first step is to calculate intermediate variables p_n and u_n using Eqs. (21) and (22). Next, we enforce the boundary condition that requires the reflected pressure to vanish at the wave-front:

$$p_-(x_{n+1}, t_{n+1}) = p_-(x_{n+1}, t_n) = 0. \tag{38}$$

Combined with Eq. (37), this boundary condition imposes the following constraint for both $m = n$ and $m = n - 1$:

$$[\varepsilon_n u_{nm} + \eta_n q_{nm}] = B_n \cdot [p_{nm} + u_{nm}] - \frac{p_-(x_n, t_m)}{c\Delta t}. \tag{39}$$

Equation (39), when applied at two points in time, provides sufficient information to calculate the two variables ε_n and η_n. Once ε_n and η_n are known, rearrangement of Eqs. (36) and (37) allows evaluation of p_+ and p_- at $x = x_{n+1}$:

$$p_+(x_{n+1}, t_{m+1}) = p_+(x_n, t_m) - \{B_n p_{nm} + [(\varepsilon_n - B_n)u_{nm} \\ + \eta_n q_{nm}]\}c\Delta t, \tag{40}$$

$$p_-(x_{n+1}, t_{m-1}) = p_-(x_n, t_m) - \{B_n p_{nm} \\ - [(\varepsilon_n - B_n)u_{nm} + \eta_n q_{nm}]\}c\Delta t, \tag{41}$$

for $m = n, \dots, t_{\max}/\Delta t$. Finally, finite-difference approximations of Eqs. (7) and (35) provide a way to calculate $A(x_{n+1})$ and $B(x_{n+1})$:

$$A(x_{n+1}) \approx A(x_n)\exp(2c\varepsilon_n\Delta t), \tag{42}$$

$$B(x_{n+1}) \approx B(x_n) + 2\eta_n\Delta t. \tag{43}$$

Successive repetition of these steps allows calculation of $A(x)$ and $B(x)$ for $0 < x \le x_{\max}$ given $p_+(0,t)$ and $p_-(0,t)$ for $0 \le t \le t_{\max}$, where $x_{\max} = t_{\max}/2\,c$.

Note that when $p_+(0,t)$ is a Kronecker delta function, $p_+(0,t) = 1$ at $t = 0$ and $p_+(0,t) = 0$ for $t \ne 0$, then $p_-(0,t)$ is, by definition, the time-domain reflectance. This makes knowledge of the time-domain reflectance at $x = 0$ over the range $0 \le t \le t_{\max}$ sufficient to calculate $A(x)$ and $B(x)$ over the range $0 < x \le x_{\max}$.

III. APPLICATION

The inverse solution has been used to generate area functions of infinite horns from their reflectance functions. Three specific horn shapes are presented as examples—parabolic, conical and exponential. Figure 1 shows the diameter as a function of axial distance x obtained for these three horns from the equations listed in Table I. In each case, the diameter is 1 cm at $x = 0$ cm and expands to make the cross-sectional area $A(10) = 10$ cm^2. Values of α required to achieve the specified area expansion are listed in Table I for all horn shapes, as are values for $\varepsilon(x)$, the logarithmic gradient of horn diameter that appears in Eq. (6).

The inverse solution described in Sec. II E was implemented using MATLAB software (MathWorks) with a sampling rate of 1 MHz. If our inverse solution is successful we
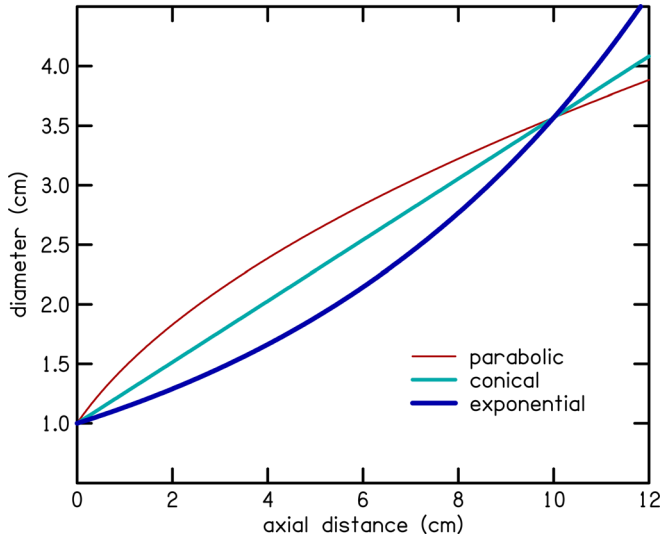
J. Acoust. Soc. Am., Vol. 131, No. 3, March 2012

Rasetshwane *et al.*: Horn inverse solution   1867

FIG. 1. (Color online) Horn diameter (D) as a function of axial distance (x) for various horn shapes. In the selected examples, the diameter is 1 cm at $x = 0$ and expands to make the cross-sectional area $A = 10$ cm^2 for all horn shapes at $x = 10$ cm.

expect the diameter functions it generates to match those shown in Fig. 1.

Frequency-domain reflectance at the entrance ($x = 0$) of the three horns are shown in Fig. 2. Specifically, Fig. 2 shows the magnitude (top panel) in decibels, the phase (middle panel) in cycles, and the group delay, defined as $\tau(\omega) = -\partial R(0, \omega)/\partial\omega$, (bottom panel) in units of ms of the reflectance. These reflectance functions were obtained from theoretical equations presented in the Appendixes, i.e., Type-I reflectance. Some useful information can be drawn from the frequency-domain reflectance. The arrow at a frequency of $f_c = 694$ Hz shows what is referred to as the cutoff frequency of the exponential horn. The cutoff frequency is related to α by $f_c = \alpha c/2\pi$. Below f_c the reflectance magnitude is 0 dB (or nearly 0 dB for the parabolic and conical horns), which indicates complete (or nearly complete) reflection, so there is no wave propagation. Above the cutoff the reflectance magnitude has a slope of about -20 dB/decade and there is wave propagation. For this reason, horns are sometimes characterized as high-pass lines, in analogy to high-pass filters. The non-constancy of the reflectance above f_c tells us that wave propagation is dispersive, i.e., depends on frequency. The group delay is greater than zero at all frequencies for all the horns, suggesting that the reflectance is

TABLE I. Horn diameter and its logarithmic gradient for various horn shapes. The value of α was selected (for parabolic, conical, and exponential horns) to make area $A(10) = 10$ cm while diameter $D(0) = 1$ cm. The units of α and ε are cm^{-1}, while the unit of D is cm.

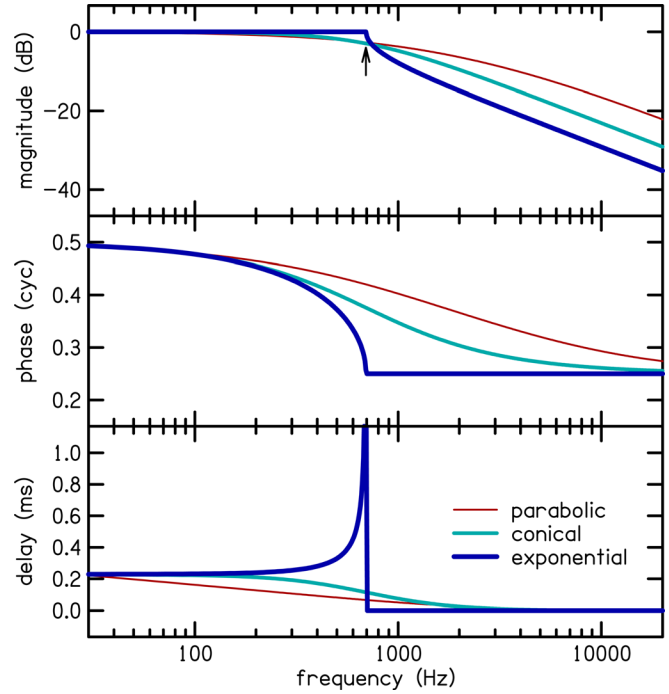|	α	$D(x)$	$\varepsilon(x)$
uniform	—	1	0
parabolic	1.173	$\sqrt{1 + \alpha x}$	$\dfrac{1}{2}\dfrac{\alpha}{1 + \alpha x}$
conical	0.257	$1 + \alpha x$	$\dfrac{\alpha}{1 + \alpha x}$
exponential	0.127	$\exp(\alpha x)$	α

FIG. 2. (Color online) Reflectance in the frequency-domain $R(0, 2\pi f)$. The reflectance functions were obtained from theoretical equations presented in the Appendixes. The arrow indicates the cutoff frequency.

causal. The group delay for the exponential horn is highest near the cutoff frequency.

Time-domain reflectance was obtained from frequency-domain reflectance by using the inverse Fourier transform. Figure 3 shows the time-domain reflectance (solid lines) for the three horns. The inverse Fourier transforms were
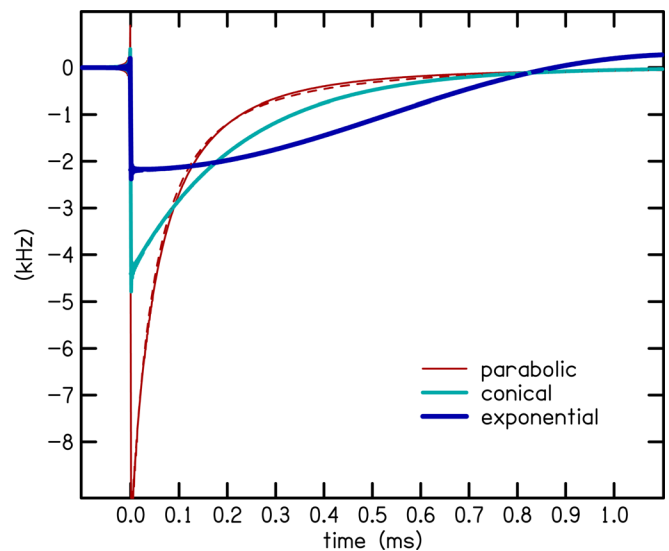

FIG. 3. (Color online) Reflectance in the time domain. The inverse Fourier transforms of frequency-domain reflectance were multiplied by the sampling rate to display values that are independent of sampling rate (solid lines) and are superimposed over the expressions for time-domain reflectance $r(0,t)$ that are presented in the Appendixes (dashed lines). Good agreement between these two sets of curves completely obscures the dashed lines except for the parabolic horn. The inverse solution used only the time-domain reflectance calculated by inverse Fourier transform.
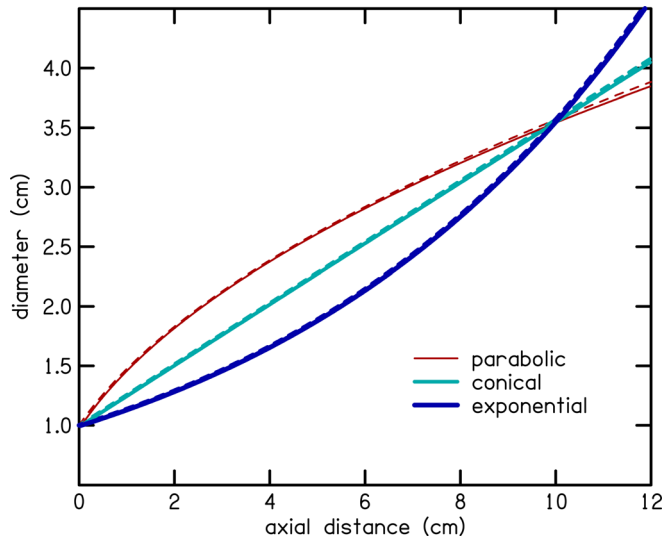
FIG. 4. (Color online) Horn diameter inverse solution (solid lines) compared with true values (dashed lines), which were calculated from the expressions listed in Table I. The curves in this figure represent $D(x)$.

FIG. 5. (Color online) Horn inertance $B(x)$ inverse solution (solid lines) compared with $\varepsilon(x)$ (dashed lines), which was calculated from the expressions listed in Table I. The agreement between $B(x)$ and $\varepsilon(x)$ was unexpected.

multiplied by the sampling rate in order to display reflectance values that are independent of sampling rate. For comparison, the dashed lines represent explicit expressions for the time-domain reflectance presented in the Appendixes. Good agreement between these two sets of curves completely obscures the dashed lines except for the parabolic horn, where the expression for time-domain reflectance is only approximate. The time-domain reflectance functions obtained from the inverse Fourier transform display some oscillatory behavior near $t = 0$. This "ringing" artifact is a form of Gibbs phenomena due to restriction of the frequency-domain reflectance to a finite bandwidth. Theoretically, time-domain reflectance should be causal (i.e., zero for $t < 0$).

To generate an area function using our inverse solution requires the knowledge of $p_+(0,t)$, $p_-(0,t)$, and $A(0)$. $A(0)$ can be obtained from measurement of $Y_0 = A(0)/\rho c$ and using $A(x) = \pi(D(x)/2)^2$. We selected $p_+(0,t)$ to be a delta function and, by definition, when $p_+(0,t)$ is a delta function, $p_-(0,t) = r(t)$, the time-domain reflectance. Figure 4 shows diameter functions (solid line) for the three horns obtained from the inverse solution with initial parameter values selected as described. The diameter functions obtained from equations listed in Table I are also plotted as dashed lines for comparison. The match is very good, except above $x \approx 8$ cm where the generated diameter functions for the parabolic and conical horn deviate slightly from the true values.

The solid lines in Fig. 5 represent values of $B(x)$ that were calculated along with $A(x)$ as part of the inverse solution. For comparison, the dashed lines represent the logarithmic gradient of the horn diameter $\varepsilon(x)$. The numerical agreement between B and ε was unexpected and suggests that $b(x) = \varepsilon(x)$. However, we have no proof that this relation generalizes to all horn shapes.

Figures 1–5 showed results for application of our inverse solution to horns with $A(x)$ that increase with increasing x. Our inverse solution also works well for an exp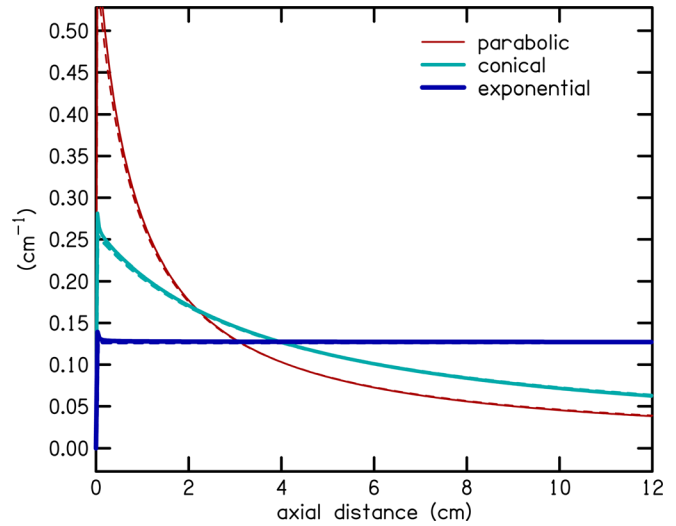onential horn with decreasing $A(x)$. This horn is still an infinite horn since $A(x)$ never equals zero as x increases, it only approaches zero. Our inverse solution works for the decreasing exponential horn because the reflectance magnitude still asymptotes to $1/f$ as $f \to \infty$. For the parabolic and conical horns with decreasing $A(x)$, $A(x) = 0$ at some finite value of x, which causes reflectance magnitude to not approach zero as $f \to \infty$. Although our solution method may be extended to finite-length horns by applying a frequency-domain window to the reflectance, no such results are presented in this paper.

Simulation results were obtained for the exponential with decreasing $A(x)$. The frequency-domain reflectance magnitude and delay for this horn (not shown) are identical to those of the exponential horn with increasing $A(x)$. The phase of the former is shifted by one-half cycle relative to that of the latter at all frequencies. The time-domain reflectance of the exponential with decreasing $A(x)$ (not shown) is a mirror image of the time-domain reflectance of the exponential with increasing $A(x)$ about the ordinate zero. Figure 6 shows the diameter function (solid line) for the exponential horn with decreasing $A(x)$ obtained from the inverse solution. The diameter functions obtained from $D(x) = e^{-\alpha x}$ is also plotted as dashed lines, for comparison. The match is very good. Horn diameter inverse solution and true values for the exponential horn with increasing $A(x)$ (presented in Fig. 4) are reproduced in Fig. 6 for comparison.

IV. DISCUSSION

The formulation of our inverse solution is based on Webster's horn equation, which assumes lossless plane-wave propagation. We chose to restrict our solution to Webster's horn equation because exact solutions are available. In actual physical horns, wave propagation is not one-dimensional; higher order modes (HOM) of wave propagation are present at high frequency or when the diameter of the horn is no longer small compared to the wavelength of the propagating wave. Webster's horn equation does not
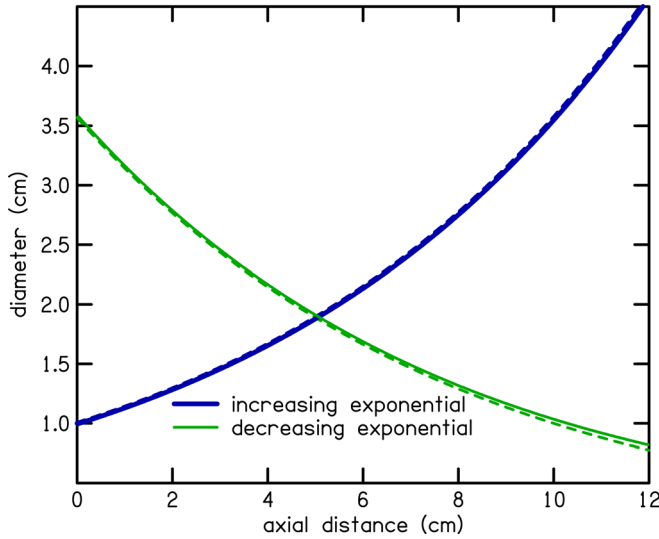
FIG. 6. (Color online) Horn diameter inverse solution (solid lines) compared with true values (dashed lines) for exponential horn with decreasing area function. The diameter functions obtained from $D(x) = e^{-\alpha x}$ is also plotted as dashed lines, together with reproductions of increasing diameter function of Fig. 4 for comparison. The curves in this figure represent $D(x)$.
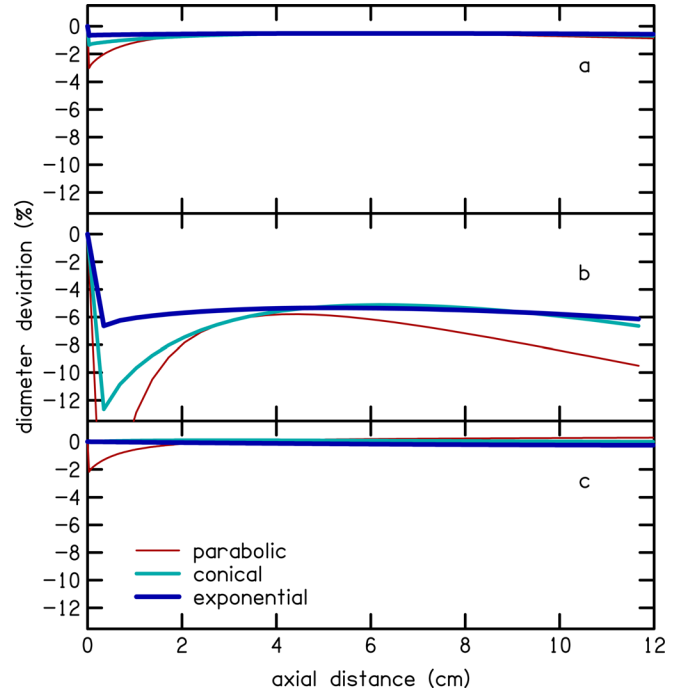

FIG. 7. (Color online) Evaluation of the limitations of the inverse solution. (a) A sampling rate of 1 MHz results in good diameter estimation and computational efficiency. (b) Decrease of the sampling rate to 100 kHz results in increased diameter deviation. (c) Using Type-II reflectance at $x = 0$ reduces the diameter deviations but makes the inverse solution less stable.

account for HOM and therefore cannot accurately describe wave propagation (Morse and Feshbach, 1953, p. 1352). In addition to HOM, there are viscous and thermal propagation losses in physical horns. Under these conditions, the current formulation of our solution to the inverse problem will produce errors in the area functions obtained. It may be possible to improve the accuracy of our inverse solution by using horn equations that better model the geometry of wave propagation, such as the curvilinear horn equation (Agullo et al., 1999), and by modeling for viscous and thermal losses (following, e.g., Keefe, 1984).

Our solution to the inverse problem recasts Webster's horn equation in terms of forward and backward traveling pressure waves obtained through the decomposition of the total acoustical pressure. This decomposition is important since the definition of reflectance itself relies on these definitions of wave variables, and may provide further insights into the meaning of reflectance. Wave variable decomposition has also been shown to facilitate the computation of a less complex and more stable impulse responses in modeling of the bore of wind instruments (e.g., Martinez et al., 1988).

To explore limitations of our inverse solution, we examined the influence on its accuracy of two variations in the method: (1) lower sampling rate and (2) alternate boundary condition at $x = 0$. Deviation of the reconstructed diameter from the actual diameter for the results described above [with a sampling rate 1 MHz and $B(0) = 0$] is about 0.5% at 5 cm from the horn entrance [see Fig. 7(a)]. When the sampling rate is decreased by a factor of 10 (to 100 kHz), the diameter deviation increases by about a factor of 10 for all three horns [see Fig. 7(b)]. When the sampling rate is increased by a factor of 10 (to 10 MHz), the diameter deviation decreases by about a factor of 5 for conical and parabolic horns, but doubles for the exponential horn at 10 cm from the entrance (not shown).

When the sampling rate is 1 MHz, much of the error in the inverse solution is apparently due to the discontinuity in $B(x)$ at $x = 0$. This discontinuity could be removed by setting $B(0) = b(0)$, which specifies Type-II reflectance at the horn entrance instead of Type-I reflectance. However, this approach fails for the parabolic horn because Type-II reflectance is not causal. As a compromise, we can specify $B(0)$ in a way that removes as much of the TDR step as possible, while still remaining causal:

$$B(0) = \min_{\omega > 0} \Re\left\{\frac{i\omega}{c}\left[\frac{Y_r(0, \omega)}{Y_0(0)} - 1\right]\right\},\qquad(44)$$

where $\Re$ denotes the real part. This equation selects $B(0) = b(0)$ for the exponential and conical horns and $B(0) < b(0)$ for the parabolic horn. The diameter deviation is reduced by this boundary condition for all three horns [see Fig. 7(c)]. However, the inverse solution is apparently less stable for this boundary condition because the inverse solution fails for all three horns when the sampling rate is reduced to 100 kHz. For this reason, the boundary condition $B(0) = 0$ seems to be the best choice.

Our definition of Type-II reflectance, which subtracts the step admittance from the radiation admittance, was previously suggested (with different notation) by Farmer-Fedor and Rabbitt (2002) in the context of horn acoustics. However, they did not use Type-II reflectance to obtain an inverse solution and made no notice of the fact that Type-II reflectance is non-causal for horn profiles with negative curvature.

Although our definition of Type-II reflectance introduces new concepts, such as step admittance Y_s and horn

inertance B, these terms are useful in imposing a condition of continuity on TDR for non-uniform horns, and thereby facilitate a functional inverse solution with reasonably accurate results. Although we attempted to derive an inverse solution in terms Type-I reflectance, to alleviate concerns about the non-causality of Type-II reflectance, these attempts were unsuccessful. Continuity in the wave variables is apparently essential to the inverse solution, while causality (of reflectance) is only required at the horn entrance.

We were surprised to observe (for the three horn shapes we studied) that $B(x) = \varepsilon(x)$ for $x > 0$. We suspect that this relationship holds for all horn shapes; however, we are unable to provide a mathematical proof at this time. Our hybrid approach of using Type-I reflectance at $x = 0$ and Type-II reflectance for $x > 0$ allows a solution without requiring such a proof This boundary condition at $x = 0$ represents a "matched" acoustic source in that reverse propagating waves are not reflected back at $x = 0$. In practical measurement situations, the surge admittance $Y_0(0)$ can be estimated from the measured radiation admittance $Y_r(0)$ at the horn entrance and provides sufficient information for estimating horn profiles (i.e., diameter functions) according to our inverse-solution method.

The definition of reflectance for finite-length horns requires additional consideration of the boundary condition at the location where the horn terminates. When this boundary condition is expressed as a termination admittance Y_t, such that $Y_r = Y_t$ at the termination point, then it is of interest to know what value of Y_t minimizes reflection from this point. We derived the termination admittance by setting our expression for the backward travelling wave variable, Eq. (18), to zero to obtain

$$Y_t(L, \omega) = Y_o(x)\left[1 + \frac{\varepsilon(x)}{\kappa(\omega)}\right],\tag{45}$$

where $\varepsilon(x) = B(x)$ and $\kappa(\omega) = \frac{i\omega}{c}$. If $P_-(L, \omega) = 0$ for a length L horn, then there is no reflection at the termination of the horn. We refer to the admittance of Eq. (45) as the wave variable (WV) terminal admittance. In a numerical simulation solving a finite-difference approximation of the second-order horn equation, we observed that terminating an exponential horn with the WV terminal admittance results in less reflection when compared to terminating with the characteristic admittance Y_0. Examples of root-mean-square of the time-domain reflectance computed over an interval that includes the reflected wave are (0.079, 0.131, 0.197 0.333) $\times 10^{-3}$ for termination with WV and (0.102, 0.214, 0.395, 0.773) $\times 10^{-3}$ for termination with Y_0 for $L = 12, 24, 48$ and 96 cm. Our observation that the WV admittance provides a better admittance match at the horn termination than Y_0 supports the validity of the WV decomposition, independent of the inverse solution.

Historical interest in solutions of the inverse problem for determination of vocal tract shape was reviewed in Sec. I. Another potential application of the inverse solution is in estimation of ear canal shape from measurements of reflectance. However, the current solution method does not work well when the bandwidth of the measured reflectance

extends beyond the Nyquist frequency (i.e., half the sampling rate). Ear canal reflectance measurements are increasingly being made for clinical purposes but sampling rates are typically less than 48 kHz and estimates of ear-canal admittance are error prone even within the limited bandwidth from 20 Hz to 20 kHz. Ear canal reflectance is not a decreasing function of frequency over this range of frequencies due to reflection of incident pressure at the eardrum. For these reasons, additional signal processing steps are necessary when the inverse solution described here is used to determine ear-canal shapes. The signal processing steps required for application of the inverse solution to actual data are beyond the scope of this article. However, preliminary results have shown good agreement between average ear-canal area function obtained with the current method and previous reports (Rasetshwane and Neely, 2011).

The two, first-order differential equations that describe a one-dimensional transmission line, long-wave model of the cochlea (e.g., Zweig *et al.,* 1976), can be expressed in the frequency-domain as

$$\partial_x P(x, \omega) = -Z_f(x, \omega)U(x, \omega),\tag{46}$$

$$\partial_x U(x, \omega) = -Y_b(x, \omega)P(x, \omega),\tag{47}$$

where $P(x,\omega)$ is the scala fluid pressure and $U(x,\omega)$ is the longitudinal volume velocity. $Z_f(x, \omega) = 2i\omega\rho_0/A_s(x)$ is the fluid impedance, where $A_s(x)$ is the cross-sectional area of the fluid chambers—the scala vestibuli and scala tympani—with fluid density ρ_0. $Y_b(x, \omega) \approx i\omega/K(x)$ is the basilar membrane (BM) admittance, where $K(x)$ is the stiffness of the BM. The horn equations of Eqs. (4) and (5) can be written in the frequency-domain using an expression that is analogous to Eqs. (46) and (47):

$$\partial_x P(x, \omega) = -\frac{\rho s}{A(x)}U(x, \omega),\tag{48}$$

$$\partial_x U(x, \omega) = -\frac{A(x)i\omega}{\rho c^2}P(x, \omega),\tag{49}$$

where $P(x,\omega)$ and $U(x, \omega)$ are the Fourier transforms of $p(x,t)$ and $u(x,t),$ respectively.

Given the similarity between the transmission line model of the cochlea [Eqs. (46) and (47)] and the horn equations [Eqs. (48) and (49)], and the success of our inverse solution in obtaining the $A(x)$ parameter of the horn equations, one can expect that it may be possible to apply our inverse solution to obtain $A_s(x)$ and $K(x)$ when an input to the stapes end the cochlea is known. This is an interesting application and possible extension of the current inverse solution. Allen (1979) derived the cochlear input impedance for frequencies less than the characteristic impedance (CF). An extension of this approach would be the application of inverse-solution methods to reveal mechanical properties of the cochlea based on ear-canal measurements. Sondhi (1980) investigated a similar application of the inverse problem of Sondhi and Gopinath (1971) to obtain BM stiffness from measurements of an impulse response at the stapes.

V. CONCLUSION

A solution to the inverse problem is described and used to determine the area function of various types of infinite acoustic horns from reflectance. An essential part of this solution is having a definition of reflectance that is compatible with the solution. Formulating the inverse solution in terms of reflectance may offer a better understanding of reflectance and impedance which may in turn be useful when measuring reflectance and impedance in the laboratory. Our inverse solution calculates numerical area functions with reasonable accuracy for infinite parabolic, conical, and exponential horns. We believe that our inverse solution can be adapted to be useful in practical applications, such as in estimating ear-canal shape, given measurements of ear-canal reflectance.

ACKNOWLEDGMENTS

APPENDIX A: RADIATION ADMITTANCE AND REFLECTANCE FOR THE PARABOLIC HORN

The equation expressing the diameter of the parabolic horn as a function of the axial distance is

$$D(x) = \sqrt{1 + \alpha x}. \tag{A1}$$

The logarithmic gradient of the horn diameter, as defined in Eq. (7), evaluates to

$$\varepsilon(x) = \frac{1}{2}\frac{\alpha}{1 + \alpha x}. \tag{A2}$$

The radiation admittance for the infinite parabolic horn is

$$Y_r(x, \omega) = i\frac{A(x)}{\rho c}\frac{H_1\left(-\dfrac{1 + \alpha x}{\alpha c}\omega\right)}{H_0\left(-\dfrac{1 + \alpha x}{\alpha c}\omega\right)}, \tag{A3}$$

where H_ν is the Hankel function of the first kind and order ν (Olson, 1947).

TABLE II. Radiation admittance and reflectance evaluated at $x = 0$.

	$Y_r(0, \omega)/Y_0(0)$	$R_1(0, \omega)$
uniform	1	0
parabolic	$i\dfrac{H_1(-\omega/\alpha c)}{H_0(-\omega/\alpha c)}$	$\dfrac{H_0(-\omega/\alpha c) - iH_1(-\omega/\alpha c)}{H_0(-\omega/\alpha c) + iH_1(-\omega/\alpha c)}$
conical	$1 + \dfrac{\alpha c}{i\omega}$	$-\dfrac{\alpha c}{\alpha c + 2i\omega}$
exponential	$\sqrt{1 + \left(\dfrac{\alpha c}{i\omega}\right)^2} + \dfrac{\alpha c}{i\omega}$	$-\dfrac{\alpha c + \sqrt{(\alpha c)^2 - \omega^2 - i\omega}}{\alpha c + \sqrt{(\alpha c)^2 - \omega^2 + i\omega}}$

When $x = 0$ the radiation admittance and reflectance become

$$Y_r(0, \omega) = i\frac{A(0)}{\rho c}\frac{H_1(-\omega/\alpha c)}{H_0(-\omega/\alpha c)}, \tag{A4}$$

$$R_1(0, \omega) = \frac{H_0(-\omega/\alpha c) - iH_1(-\omega/\alpha c)}{H_0(-\omega/\alpha c) + iH_1(-\omega/\alpha c)}. \tag{A5}$$

In the time domain, an approximate expression for reflectance at $x = 0$ is

$$r_1(0, t) = -\frac{\alpha c}{4}\exp\left(\frac{-\alpha c t}{2 + \dfrac{\alpha c t}{4 + \alpha c t/16}}\right). \tag{A6}$$

APPENDIX B: RADIATION ADMITTANCE AND REFLECTANCE FOR THE CONICAL HORN

The equation expressing the diameter of the conical horn as a function of the axial distance is

$$D(x) = 1 + \alpha x. \tag{B1}$$

The logarithmic gradient of the horn diameter, as defined in Eq. (7), evaluates to

$$\varepsilon(x) = \frac{\alpha}{1 + \alpha x}. \tag{B2}$$

The radiation admittance for the infinite conical horn is

$$Y_r(x, \omega) = \frac{A(x)}{\rho c}\left(1 - \frac{\alpha c}{i\omega(1 + \alpha c)}\right). \tag{B3}$$

When $x = 0$ (see Table II) the radiation admittance and reflectance become

$$Y_r(0, \omega) = \frac{A(0)}{\rho c}\left(1 + \frac{\alpha c}{i\omega}\right), \tag{B4}$$

$$R_1(0, \omega) = \frac{\alpha c}{\alpha c + 2i\omega}. \tag{B5}$$

In the time domain, an explicit expression for reflectance at $x = 0$ is

$$r_1(0, t) = -\frac{\alpha c}{2}\exp\left(\frac{-\alpha c}{2}t\right). \tag{B6}$$

APPENDIX C: RADIATION ADMITTANCE AND REFLECTANCE FOR THE EXPONENTIAL HORN

The equation expressing the diameter of the exponential horn as a function of the axial distance is

$$D(x) = e^{\alpha x}. \tag{C1}$$

The logarithmic gradient of the horn diameter, as defined in Eq. (7), evaluates to

$$\varepsilon(x) = \alpha. \tag{C2}$$

The radiation admittance of an infinite exponential horn is

$$Y_r(x, \omega) = \frac{A(x)}{\rho c}\left(\frac{\alpha c}{i\omega} + \sqrt{1 + \left(\frac{\alpha c}{i\omega}\right)^2}\right). \tag{C3}$$

When $x = 0$ (see Table II) the radiation admittance and reflectance become

$$Y_r(0, \omega) = \frac{A(0)}{\rho c}\left(\frac{\alpha c}{i\omega} + \sqrt{1 + \left(\frac{\alpha c}{i\omega}\right)^2}\right), \tag{C4}$$

$$R_1(0, \omega) = \frac{i\omega - \left[\alpha c + \sqrt{(\alpha c)^2 - \omega^2}\right]}{i\omega + \left[\alpha c + \sqrt{(\alpha c)^2 - \omega^2}\right]}. \tag{C5}$$

In the time domain, an explicit expression for reflectance at $x = 0$ is

$$r_1(0, t) = -\frac{J_1(\alpha c t)}{t}, \tag{C6}$$

where J_1 is a Bessel function of the first kind, order 1.

Agullo, J., Barjau, A., and Keefe, D. H. (**1999**). "Acoustic propagation in flaring, axisymmetric horns: I A new family of unidimensional solutions," Acustica **85**, 278–284.

Allen, J. B. (**1979**). "Cochlear models-1978," in *Models of the Auditory System and Related Signal Processing Techniques,* edited by M. Hoke and E. de Boer, Scand. Audiol. Suppl. **9**, 1–16.

Amir, N., Shimony, U., and Rosenhouse, G. (**1995**). "A discrete model for tubular acoustic systems with varying cross-section—The direct and inverse problems. Part 1: Theory," Acustica **81**, 450–462.

Bube, K. P., and Burridge, R. (**1983**). "The one-dimensional inverse problem for reflection seismology," SIAM Rev. **25**, 496–559.

Bremmer, H. (**1951**). "The W.K.B. approximation as the first term of a geometric-optical series," Commun. Pure Appl. Math. **4**, 105–115.

Caflisch, R. E. (**1981**). "An inverse problem for Toeplitz matrices and the synthesis of discrete transmission lines," Lin. Alg. Appl. **38**, 207–225.

Eisner, E. (**1967**). "Complete solutions of the Webster horn equation," J. Acoust. Soc. Am. **41**, 1126–1146.

Farmer-Fedor, B. L., and Rabbitt, R. D. (**2002**). "Acoustic intensity, impedance and reflection coefficient," J. Acoust. Soc. Am. **112**, 600–620.

Forbes, B. J., Sharp, D. B., Kemp, J. A., and Li, A. (**2003**). "Singular system methods in acoustic pulse reflectometry," Acustica **89**, 743–753.

Gopinath, B., and Sondhi, M. M. (**1971**). "Inversion of the telegraph equation and the synthesis of nonuniform lines," Proc. IEEE **59**, 383–392.

Keefe, D. H. (**1984**). "Acoustical wave propagation in cylindrical ducts: Transmission line parameter approximations for isothermal and nonisothermal boundary conditions," J. Acoust. Soc. Am. **75**, 58–62.

Keefe, D. H., Ling, R., and Bulen, J. C. (**1992**). "Method to measure acoustic impedance and reflection coefficient," J. Acoust. Soc. Am. **91**, 470–485.

Martinez, J., Agullo, J., and Cardona, S. (**1988**). "Conical bores. Part II: Multiconvolution," J. Acoust. Soc. Am. **84**, 1620–1627.

Mermelstein, P. (**1967**). "Determination of the vocal-tract shape from measured formant frequencies," J. Acoust. Soc. Am. **41**, 1283–1294.

Milenkovic, P. (**1987**). "Acoustic tube reconstruction from noncausal excitation," IEEE Trans. Acoust. Speech Signal Process. **ASSP-35**, 1089–1100.

Morse, P. M., and Feshbach, H. (**1953**). *Methods of Theoretical Physics* (McGraw-Hill, New York), Vols. I and II, pp. 1352.

Olson, H. F. (**1947**). *Elements of Acoustical Engineering* (Von Nostrand, New York), pp. 87–88.

Rasetshwane, D. M., and Neely, S. T. (**2011**). "Inverse solution of ear-canal area function from reflectance," J. Acoust. Soc. Am. **130**, 3873–3881.

Salmon, V. (**1946**). "A new family of horns," J. Acoust. Soc. Am. **17**, 212–218.

Schroeder, M. R. (**1967**). "Determination of the geometry of the human vocal tract by acoustic measurements," J. Acoust. Soc. Am. **41**, 1002–1010.

Sondhi, M. M. (**1980**). "Acoustical inverse problem for the cochlea," J. Acoust. Soc. Am. **69**, 500–504.

Sondhi, M. M., and Gopinath, B. (**1971**). "Determination of vocal-tract shape from impulse response at the lips," J. Acoust. Soc. Am. **49**, 1867–1873.

Sondhi, M. M., and Resnick, J. R. (**1983**). "The inverse problem for the vocal tract: Numerical methods, acoustical experiments, and speech synthesis," J. Acoust. Soc. Am. **73**, 985–1002.

Webster, A. G. (**1919**). "Acoustical impedance, and the theory of horns and of the phonograph," Proc. Natl. Acad. Sci. **5**, 275–282.

Zweig, G., Lipes, R., and Pierce, J. R. (**1976**). "The cochlear compromise," J. Acoust. Soc. Am. **59**, 975–982.

J. Acoust. Soc. Am., Vol. 131, No. 3, March 2012

Rasetshwane *et al.*: Horn inverse solution 1873